Spectral approach to transport in a two-dimensional honeycomb lattice with substitutional disorder

E. G. Kostadinova, C. D. Liaw, A. S. Hering, A. Cameron, F. Guyton, L. S. Matthews, and T. W. Hyde

Phys. Rev. B **99**, 024115 — Published 31 January 2019

DOI: 10.1103/PhysRevB.99.024115

Spectral approach to transport in a two-dimensional honeycomb lattice with substitutional disorder

E G Kostadinova [1], C D Liaw [1,2], A S Hering [3], A Cameron [4], F Guyton [5], L S Matthews [1], and T W Hyde [1]

[1] Center for Astrophysics, Space Physics & Engineering Research, Baylor University, Waco, TX, 76706, USA
[2] Department of Mathematical Sciences, University of Delaware, 311 Ewing Hall, Newark, DE 19716, USA
[3] Department of Statistical Science, One Bear Place 97310, Baylor University, Waco, TX, 76706, USA
[4] Department of Physics, Brigham Young University, Provo, UT 84602, USA
[5] Department of Physics, Applied Physics, and Astronomy, Rensselaer Polytechnic Institute, 110 8th St, Troy, NY 12180, USA

E-mail: Eva_Kostadinova@baylor.edu, liaw@udel.edu, Mandy_Hering@baylor.edu, adamc9900@gmail.com, guytof@rpi.edu, Lorin_Matthews@baylor.edu, Truell_Hyde@baylor.edu

Abstract. The transport properties of a disordered two-dimensional (2D) honeycomb lattice are examined numerically using the spectral approach to the 2D percolation problem, characterized by an Anderson-type Hamiltonian. In our model, disorder is represented by two parameters: a distribution of random on-site energies ϵ_i (positional disorder) and a concentration of doping energies p (substitutional disorder). The results indicate the existence of extended energy states for nonzero disorder and the emergence of a transition towards localized behavior for critical doping concentration $n_D > 0.3\%$, in agreement with the experimentally observed metal-to-insulator transition in a graphene sheet doped with hydrogen.

Keywords: spectral approach, doped graphene, 2D honeycomb lattice, Anderson localization, percolation

I. INTRODUCTION

Graphene is a single two-dimensional (2D) layer of carbon atoms arranged on a honeycomb lattice structure. Each carbon in this lattice has four bonds – one σ-bond connecting it with each of its three nearest neighbors and a fourth π-bond oriented out of plane. The hybridization of the π-bonds from all lattice sites creates conduction bands within the crystal causing its metallic properties. Since the discovery of graphene and related 2D materials [1], [2], the study of transport in the 2D honeycomb lattice has attracted considerable attention [3], [4]. Specifically, of interest to both industry and science is the question whether such 2D materials can exhibit a controllable metal-to-insulator transition (MIT). Experimentally, MIT has been observed for graphene doped

with NO_2 [5], hydrogen [6], and boron [7]. However, theoretically, there is a decades-long disagreement on the origins of conductivity in the critical 2D case. As numerically obtained predictions are sensitive to the choice of theoretical model and computational technique, comparison among the various models with experimental results is often challenging.

In the theory of Anderson localization [8], MIT occurs due to a critical amount of random disorder W_c, which can be represented by a random variation of the on-site lattice energies, assuming constant nonzero transfer energy. According to the well-established scaling approach to Anderson localization [9], any nonzero amount of such disorder in a 2D lattice leads to exponential or logarithmic[1] localization of the wave function propagating through the medium. In other words, there is no real transport in a 2D disordered lattice, which clearly contradicts the observed metallic behavior of materials like graphene. Proponents of scaling theory have suggested that graphene exhibits a localization length longer than the size of current numerical simulations, which leads to the "apparent" existence of delocalized states [11]–[13]. Another part of the physics community argues that scaling theory does not yield reliable results for all dimensions and system sizes [14], [15], and that its limitations come to play in the critical 2D case.

An alternative but related approach to the study of conductivity in disordered media is the quantum site percolation model, where one examines transport on assembly of lattice sites that are considered open (i.e., have energy $\epsilon_i = 0$) with probability p or closed (i.e., have energy $\epsilon_i = \infty$) with probability $1 - p$, while the transfer energy is kept at a constant nonzero value[2] [16]. In this problem, one is interested in the critical probability p_q below which all states are localized. Similar to the Anderson localization case, early numerical studies [17]–[19] based on finite-size scaling techniques have predicted that in the 2D quantum percolation problem, all energy states are localized unless $p_q = 1$. Later it was suggested that extended states occur for $p_q < 1$ but at energies far away from the band center ($E = 0$) [20]. Another set of physicists and mathematicians argued that transport in the 2D lattice can occur for $p_q < 1$ at all energies [21]–[24]. However, the exact value of the critical probability p_q appears to be sensitive to the applied technique.

Although there is no trivial correspondence between the critical amount of the disorder W_c in the Anderson localization problem and the critical probability p_q in the quantum percolation model, it is not surprising that the question of conductivity in a 2D material has caused similar disagreements in the communities studying both problems. In this paper, we numerically examine transport in the disordered two-dimensional (2D) honeycomb lattice using a spectral approach, which does not rely on perturbation theory or finite-size scaling. In the problem considered here, disorder is characterized by two dimensionless parameters: (i) a distribution of random on-site energies $\epsilon_i \in [-W/2, W/2]$ (positional disorder) and (ii) a concentration of doping energies p (substitutional disorder). Thus, we employ a two-parameter model of conductivity, where Anderson localization is studied on a percolation network, similar to the frameworks in [25], [26].

The spectral approach (first introduced by Liaw in [27]) is a mathematical technique that can determine the existence of extended states in infinite disordered lattices characterized by

[1] In the context of the scaling theory, the term "logarithmic localization" means that for weak disorder, the effects of localization will decrease the dimensionless conductance only logarithmically. More details on this definition can be found in [10] and the references therein.

[2] Alternatively, one can consider all lattice sites to be open and let the bonds be open or closed with a certain probability. This setup is called a *bond percolation* problem.

Anderson-type Hamiltonians. In this method, the spectrum of the Hamiltonian is decomposed into absolutely continuous (ac) and singular parts. The presence of an ac spectrum corresponds to delocalization of the wavefunction. Unlike techniques based on finite-size scaling, the spectral approach does not require restrictions on the Hilbert space or the use of boundary conditions. Thus, this technique can provide valuable insight into 2D transport problems, where theoretical predictions and experimental results often disagree. Additionally, the spectral approach has not to date directly contradicted results from methods based on finite-size scaling. Instead, it has provided complementary information on extended energy states that cannot be obtained from analysis of eigenvalues and density of states. This point is further discussed in Sec. IV B.

The spectral approach has been previously used to show that extended states exist in the 2D square, triangular, and honeycomb lattices with random on-site energies (positional disorder) selected from a rectangular probability distribution [27]–[29]. This choice corresponds to the zero-temperature Anderson localization problem (first introduced in [8]). In the present study, on-site random energies are assigned according to a modified bimodal probability distribution designed to model Anderson-type disorder on a 2D honeycomb percolation network. Our results indicate that extended energy states exist for small doping concentrations. We further confirm that the onset of the metal-to-insulator transition occurs for doping levels of $\approx 0.3\%$, as was experimentally observed in [6].

In Section II, we briefly introduce the transport problem on the 2D honeycomb lattice and provide motivation for our choice of a probability distribution for the random variables. In Section III, we present the details of the numerical simulation and the analysis of the results. In Section IV, we summarize the conclusions of this study, the limitations of the numerical technique, and the possible directions for future research. We also discuss the significance of the spectral approach as a complementary technique to scaling-based methods. Finally, the Appendix provides the details of the spectral technique and further references on the subject.

II. FORMULATION OF THE TRANSPORT PROBLEM

In the tight-binding approximation, the single-electron, noninteracting Hamiltonian on the 2D honeycomb lattice Λ has the form

$$H = \sum_{\substack{i.j\in\Lambda \\ i\neq j}} |e_i\rangle V_{ij} \langle e_j| + \sum_{i\in\Lambda} |e_i\rangle \epsilon_i \langle e_i|, \tag{1}$$

where $|e_i\rangle$ are the set of site basis vectors of the 2D space Λ, and V_{ij} is the hopping amplitude[3] between pairs of nearest neighbors. The on-site energies $\epsilon = \{\epsilon_i\}_{\,i\in\Lambda}$ form a set of independent variables chosen from an interval $[a, b]$ according to a prescribed probability density distribution $\chi(\epsilon)$. The probability that ϵ_i is selected from any subinterval $[a', b'] \in [a, b]$ is given by the area under the curve between the points a' and b', that is,

$$A = \int_{a'}^{b'} \chi(\epsilon) d\epsilon. \tag{2}$$

[3] The hopping amplitude represents the kinetic energy term allowing electron transport, or *hopping*, between nearest neighbor lattice sites.

Assume the on-site energies in the unperturbed crystal are constant (say, zero) and that the hopping amplitudes are taken to be constant (here $V_{ij} = 1$) between nearest-neighbor lattice sites and zero otherwise. Then, assigning the variables $\{\epsilon_i\}$ to the lattice sites corresponds to introducing disorder into the crystal, such as the positional disorder caused by deviations from lattice periodicity. If the area A defined in (2) is normalized to unity, then every lattice site is assigned an energy value from the prescribed $\chi(\epsilon)$. In this formulation, the amount and type of disorder can be varied by changing the width of the interval $[a, b]$ and the shape of $\chi(\epsilon)$, respectively.

For sufficiently large number of lattice sites and the assumption of independent random impurities, the probability distribution $\chi(\epsilon)$ in a single-species crystal approaches a Gaussian function (Fig. 1a) due to the central limit theorem. In the presence of a second atomic species, it is convenient to use the bimodal distribution (Fig. 1b), which consists of two continuously connected Gaussian peaks

$$\chi(\epsilon_i) = pf(\epsilon_i - E_A) + (1-p)f(\epsilon_i - E_B), \tag{3}$$

where

$$f(\epsilon_i - E_A) = \frac{1}{\sqrt{2\pi\sigma_A^2}} exp\left[-\left(\frac{\epsilon_i - E_A}{2\sigma_A^2}\right)^2\right] \tag{4a}$$

and

$$f(\epsilon_i - E_B) = \frac{1}{\sqrt{2\pi\sigma_B^2}} exp\left[-\left(\frac{\epsilon_i - E_B}{2\sigma_B^2}\right)^2\right]. \tag{4b}$$

In this case, the mixing parameter p corresponds to the concentration (fraction) of A-atoms, while $(1-p)$ is the concentration of B-atoms. For appropriate choices of mixing parameter p and characteristic energies E_A and E_B, the bimodal distribution can be used to study the transport properties of a binary alloy. In this approach, the amount of disorder in the system can be controlled by variation of the difference $|E_B - E_A|$, the width of the standard deviations σ_A and σ_B, and / or the mixing parameter (concentration) p.

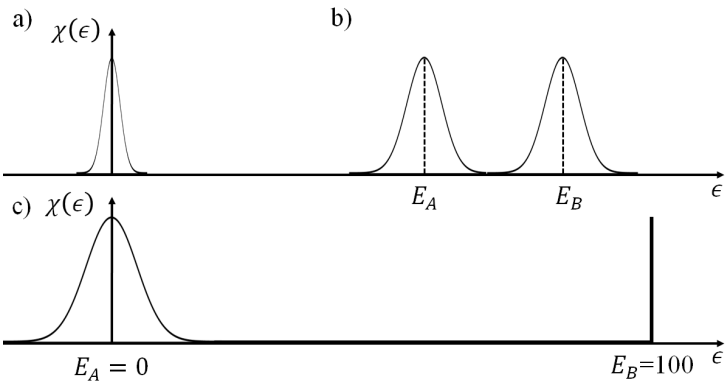

FIG. 1. Graphs of the a) Gaussian, b) bimodal, and c) modified bimodal probability density distributions as discussed in the text. Note that the distribution in c) is obtained from that in b) by keeping the width of one Gaussian fixed and shrinking the width of the other so that the latter approaches a delta function. Thus, although the two peaks have large separation, they still form a continuous distribution function.

A limiting case of the binary alloy model is obtained when the Gaussian functions from equation (3) are substituted with delta peaks and one lets $|E_B - E_A| \to \infty$ (the strong scattering limit) [17], [30]–[32]. This yields a distribution of the form

$$\chi(\epsilon_i) = p\delta(\epsilon_i - E_A), \tag{5}$$

where $\delta(\epsilon_i - E_A)$ is the delta function. In this formulation of the problem, the A-type atoms are open (perfect acceptors) with some probability p, while the B-type atoms are closed (perfect barriers) with probability $1-p$. Thus, transport occurs only on a random assembly of A-type atoms, and the existence of extended or localized clusters depends only on the fraction p. Here we introduce two modifications to this transport model: (1) let the A-type atoms be represented by a Gaussian (instead of delta) function peaked at low energy and (2) let the B-type atoms be represented by a delta function peaked at high (but finite) energy. In this new formulation, transport occurs on a random assembly of *imperfect* A-type acceptors in the presence of *imperfect* B-type barriers. This choice for energy distribution is motivated by the specific problem at hand – a 2D graphene sheet doped with atomic hydrogen.

Doped lattices can be viewed as an intermediate scenario between the binary alloy approach and models based on the strong scattering assumption. In this case, most lattice sites are occupied by A-type atoms and only a small fraction of lattice sites ($1\% \lesssim$) are occupied by B-type atoms. The A-type atoms can exhibit randomness of the on-site energies (positional disorder), while the B-type atoms represent a controlled fraction of energy states that are unfavorable but not forbidden (substitutional disorder). To study this scenario, we use a modified bimodal distribution for the on-site energies, which consists of one Gaussian peak centered around E_A and one delta function peak located at E_B (Fig. 1c). The amount of substitutional disorder is numerically controlled by the width of the Gaussian and the doping concentration is varied by assigning the value E_B to a fraction $(1-p)$ of lattice sites. Thus, this is a two-parameter transport problem.

III. NUMERICAL WORK

In mathematical terms, the time evolution of the system dynamics is determined by the Hamiltonian operator H, which reflects the potentials and interactions in the medium. Given the initial energy state, call it v_0, and constraints of the examined problem, the state at any subsequent time can be obtained upon iterative application of H on the initial state. The time evolution of the system dynamics is then given by the sequence $\{v_0,\ H_\epsilon v_0,\ (H_\epsilon)^2 v_0,\ \cdots, (H_\epsilon)^N v_0\}$, where N is the number of timesteps. In the spectral method, one calculates the mathematical distance D from *any other vector* in the Hilbert space, call it v_1, to the sequence $\{v_0,\ H_\epsilon v_0,\ (H_\epsilon)^2 v_0,\ \cdots, (H_\epsilon)^N v_0\}$. It can be shown that transport in the form of extended energy states exists if D approaches a nonzero value as time goes to infinity, i.e., if $\lim_{N\to\infty} D > 0$. The basic steps in the spectral method applied to the special case of a disordered 2D honeycomb lattice Λ are outlined in the Appendix. Definitions of the mathematical concepts used in the Appendix, such as cyclicity and spectral decomposition, can be found in [27], [28], [33]. These references also provide detailed proofs and a physical interpretation of the spectral approach. A comparison between the spectral technique and scaling theory is discussed in Sec. IV B.

In all simulations presented here, we apply the spectral technique to the discrete random Schrödinger operator

$$H_\epsilon = -\mathrm{ZV} + \sum_{i\in\Lambda} \epsilon_i e_i \langle e_i|, \tag{6}$$

where we assume that the Laplacian is given by $\Delta = ZV$ (i.e., constant hopping amplitudes V over the nearest neighbors Z), and let $\{e_i\}_{i\in\Lambda}$ be the standard basis vectors of the honeycomb lattice, such that e_i assumes the value 1 in the i^{th} entry and zero in all other entries. The numerical analysis starts by generating one realization of the random variables ϵ_i according to the prescribed modified

bimodal distribution $\chi(\epsilon)$. Next, a random base vector e_0 is selected as the initial state and used to produce the sequence $\{e_0, He_0, H^2e_0, \ldots, H^Ne_0\}$, where $N = 4500$[4]. At each timestep, the corresponding distance value $D^N_{\epsilon,W}$ is obtained using equation (13) from the Appendix. Finally, the graph of $D^N_{\epsilon,W}$ vs. N is analyzed to determine the limiting behavior of $D^N_{\epsilon,W}$ as $N \to \infty$.

The use of the modified bimodal distribution for the random variables $\{\epsilon_i\}$ allows for introduction of two distinct types of defects: positional and substitutional. The positional disorder is controlled by the variance σ^2 of the Gaussian peak[5], while doping is achieved by variation of the concentration[6] n_D of B-type lattice sites of energy E_B. In Sec. III A, we provide motivation for the choice of the distribution variables E_A, E_B, and σ^2 by examining their effect on the outcomes of the spectral method. In Sec. III B, we fix these parameters and explore the influence of increasing the doping n_D on the transport behavior of the 2D honeycomb lattice.

A. Distribution variables

In the present numerical analysis, we use a modified bimodal distribution, which consists of a single Gaussian peak centered at energy $E_A = 0$ and a delta function peak centered at energy $E_B = 100$ (Fig. 1c). Since the introduction of substitutional disorder in a material is usually a controlled process, we do not consider a spread of possible energies for the B-type atoms. Instead, the B-type atoms are represented by a delta function peaked at high average energy E_B. In other words, the doping is produced by a careful substitution of an A-type atom with a B-type atom, where E_B is controlled. The necessary condition for the numerical construction of a two-species lattice is that $E_B > 2ZV$, where Z is the number of nearest neighbors and V is the constant hopping potential [30]. This ensures that the on-site energies are well represented by a bimodal distribution (i.e., the two peaks or sub-bands centered about the values E_A and E_B do not overlap). For the honeycomb lattice ($Z = 3$) with a unit hopping potential ($V = 1$) we obtain $2ZV = 6 \ll 100 = |E_B - E_A|$, which shows that this choice of parameters is reasonable.

1. Choice of $\epsilon = 0$ for the unperturbed energies

Even in the zero-temperature unperturbed crystal, an electron wavefunction will be extended for energies within the band and localized for energies within the band gap. Thus, it is logical to expect that, as disorder is increased in the system, the lattice sites with energies closest to the band gap will be excluded from the band faster than the state $\epsilon = 0$ at the center of the band. Here we assume all unperturbed lattice sites have energy $\epsilon = 0$ (neglecting the finite width of the unperturbed band) based on the following arguments.

Physically, due to Pauli exclusion principle, the on-site energies of an infinite unperturbed lattice form a continuous band. The width of the unperturbed energy band and the corresponding statistics are sensitive to the number of lattice sites. In a macroscopic piece of material, the number of atoms is $\sim 10^{22}$, while in the present numerical simulation we have $\sim 4 \times 10^7$ lattice sites. Thus, in our case, a numerically generated continuous band can only be approximated if the assigned energy values are closely spaced, i.e., the width of the band is very narrow. Since the variation of energy

---

[4] Note that N is the number of times H acts on the initial state. Thus, it represents the timestep and not the number of lattice sites, which is $\approx 4 \times 10^7$ for the given geometry.

[5] In the following sections, we let $\sigma_A^2 \to \sigma^2$ for notational simplicity.

[6] Here n_D stands for the concentration of the B-type doping material and is equal to the probability for a closed barrier $1 - p$ in the percolation graph.

in such narrow band is much smaller than the energy differences representing disorder, we expect that their influence on the transport behavior can be neglected.

In our simulations, we start by generating a matrix of zeros (representing the lattice). At the initial timestep we assign the value 1 to a matrix element at the center of the matrix. This corresponds to positioning the electron at the center of the lattice. Then, we introduce impurities by selecting random numerical values from the interval $[-W/2, W/2]$ (W represents the magnitude of the disorder) and assigning them according to a Gaussian PDF to each lattice site, including the one where the electron is located initially. In other words, every lattice site gets a numerical value ϵ_i, which represents its on-site potential. In each following timestep, the electron wavefunction is propagated through the lattice by adding a fraction ϵ_i/Z to all the nearest neighbors (Z being the number of nearest neighbors) and subtracting the value ϵ_i from itself. The magnitude of the fraction assigned to any lattice site is dependent on the corresponding on-site potential ϵ_i. The probability for the electron to spread does not depend on the average magnitude of the initially assigned energies but instead on the energy variations among neighboring sites. If all lattice sites (including the one representing the initial state) have similar energy values, the resulting transport behavior will be delocalized. However, as the energy variation among neighboring sites increases, the resulting transport behavior will be localized, unless some other type of hopping / correlation is assumed. Thus, if the initial on-site energies did not have $\epsilon = 0$, but instead, had some slightly different constant energies $\{\epsilon_i^0\}$, the result would be an overall constant increase in the initial mean energy of all lattice sites. In our setup, the lattice site where the traveling electron is located initially will gain a constant energy increase of the same order of magnitude as the initial energies assigned to the other lattice sites. This will not have appreciable effect on the overall transport behavior.

2. Choice of mean $E_A = 0$ for the Gaussian

It has been argued that for a bipartite graph (such as the one examined here), if the center of the band is symmetrically distributed around $E_A = 0$, then the states with $\epsilon = 0$ are the only ones to not become localized. To examine how the inclusion of the $\epsilon = 0$ energy states affects delocalization, we applied the spectral approach to a 2D honeycomb lattice where the variance is fixed with $\sigma^2 = 0.4$ and the mean energy is varied within the ranges $E_A \in [0,2]$ (where the value $\epsilon = 0$ is included) and $E_A \in [20,100]$ (where the value $\epsilon = 0$ is excluded)[7]. In each numerical calculation, we let the Gaussian tails extend to four standard deviations in each direction. Thus, for $\sigma^2 = 0.4$, we have $\sigma = \sqrt{0.4} \approx 0.63$, which means that the range of allowed energy values in each calculation is $8 \times 0.63 = 5.04$ (see Fig.2). If the mean is $E_A = 0$, the calculation will include all energy values in the range $[-2.52, 2.52]$. Thus, if the mean is chosen to be bigger than 2.52 or smaller than -2.52, the corresponding range of energies will exclude the value $\epsilon = 0$.

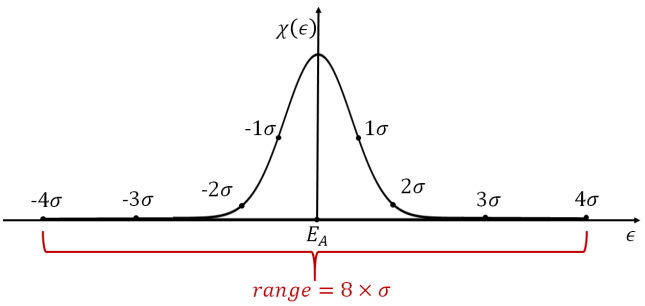

FIG. 2. Range of allowed energy values in each numerical calculation.

[7] Due to the symmetry of the Gaussian distribution, the same analysis can be performed for variation of the mean in the negative range of energy values.

As we increase the mean from 0 to 2, the position of the value $\epsilon = 0$ shifts from the center of the Gaussian towards the tails, which implies that the likelihood of having on-site states with $\epsilon = 0$ decreases. In Fig. 3 a), b), and c) we see that the corresponding distance values do not show appreciable deviation from the case $E_A = 0$, which happens if the observed delocalized behavior is due to the concentration of states with energy $\epsilon = 0$. This point is further confirmed by Fig. 3 d), where we consider realizations with mean far away from $E_A = 0$.

These observations agree with the following mathematical reasoning: changing the mean of the Gaussian distribution from $E_A = 0$ to $E_A \neq 0$ amounts to shifting the energy spectrum by a constant value, which only matters if one is interested in studying the localized behavior. In other words, assume we have all spectral information for some operator like the Anderson-type Hamiltonian H_ϵ, where the on-site energies are chosen from a PDF centered around $E = 0$. In the localized regime, this yields the eigenfunction-eigenvalue pair φ, λ, so that $H_\epsilon \varphi = \lambda \varphi$. Now shifting the mean form $E = 0$ to some constant value $E = s$ results in adding the constant s to all diagonal elements in H_ϵ and is, therefore, equivalent to using the shifted Hamiltonian $H'_\epsilon = H_\epsilon + s\, I$, where I is the identity operator. The resulting spectrum is given by $H'_\epsilon \varphi = (H_\epsilon + s\, I)\varphi = (\lambda + s)\varphi$, i.e., the same eigenfunctions are preserved but the eigenvalues are shifted by the constant s. In the delocalized regime, the existence of extended states corresponds to a continuous component of the energy spectrum, which is not affected by such a shift.

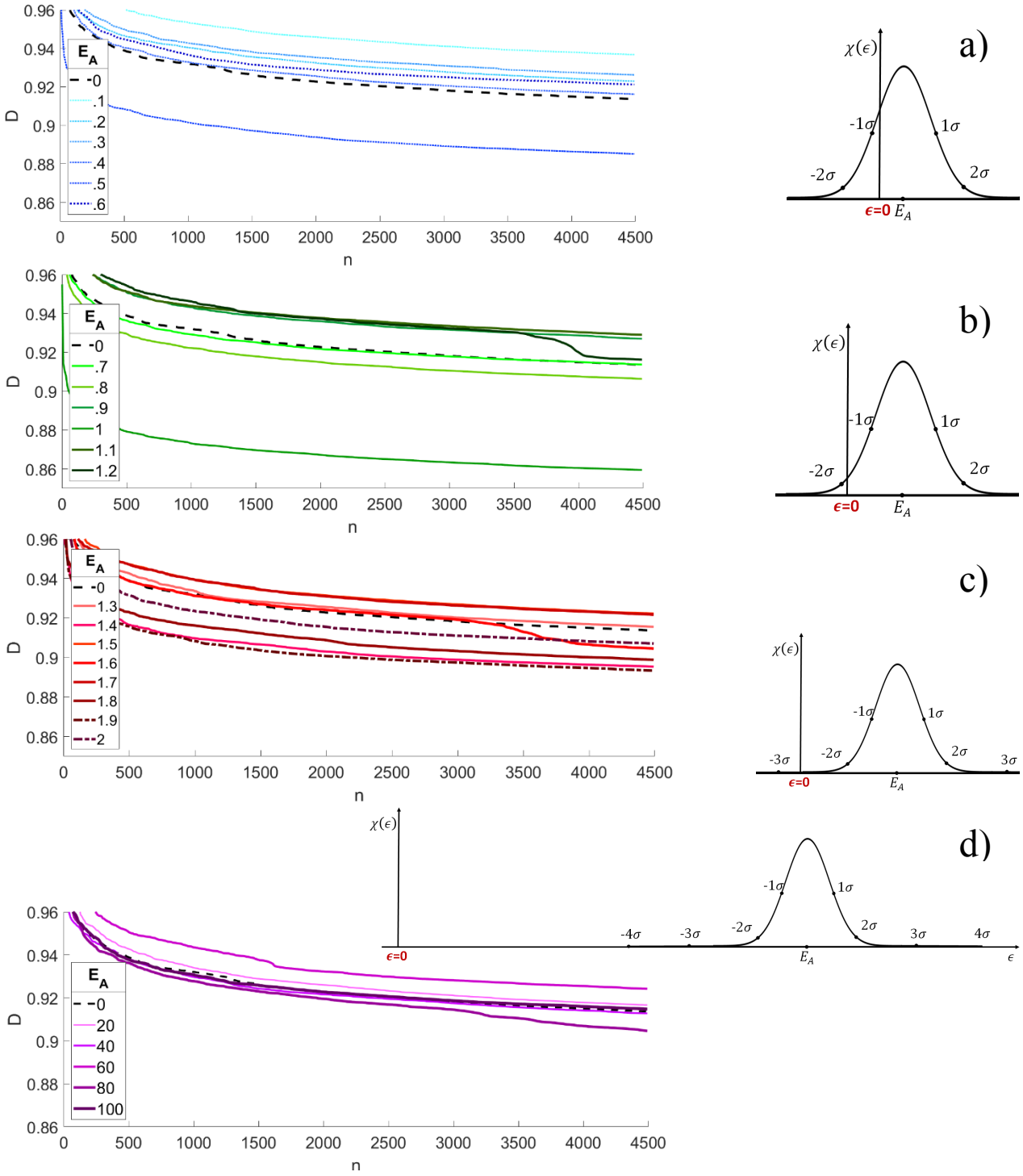

FIG. 3. D-plots generated assuming a Gaussian distribution of the on-site energies with variance $\sigma^2 = 0.04$ and mean selected from the range a) $E_A \in [0,0.6]$, b) $E_A \in [0.7,1.2]$, c) $E_A \in [1.3,2]$, d) $E_A \in [20,100]$. For each range, the realization corresponding to $E_A = 0$ is shown as a black dashed line. The smaller plots next to each graph show the characteristic position of the value $\epsilon = 0$ for each range of energy values.

2. Choice of the variance $\sigma^2 = 0.05$ for the Gaussian

To evaluate how changing the variance σ^2 influences the transport behavior of a system, we applied the spectral method to lattices generated using a Gaussian distribution with mean $E_A = 0$ and variance within the range $\sigma^2 \in [0.05,0.50]$. The distance plots in Fig. 4a show that as the variance is increased, the slopes become increasingly negative. Since delocalization in the spectral approach is established when the distance parameter approaches a nonzero value as time goes to infinity (see Appendix), the existence of extended states is more likely for plots which quickly approach a zero slope. In contrast, as the slope of the D_{hc}-plots becomes increasingly negative, the likelihood of $D_{hc}(\infty) > 0$ decreases. To quantify this reasoning, we require that delocalization can be claimed for plots that flatten exponentially for the given number of timesteps ($N = 4500$). In Fig. 4b, we see that for $\sigma^2 \leq 0.15$, the log-log D_{hc}-plots are straight lines with almost no slope, which indicates exponential decay, while for $\sigma^2 > 0.15$, the negative slope of the lines monotonically increases with increasing σ^2.

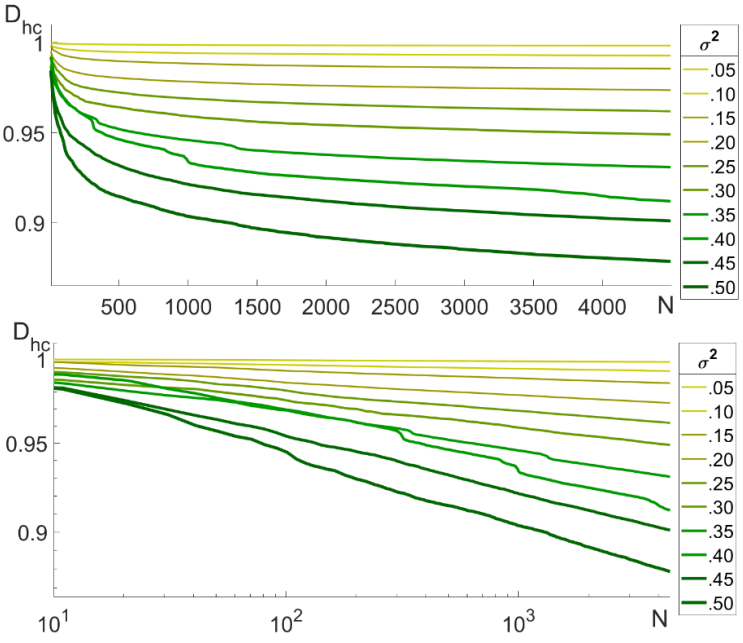

FIG. 4. Distance time evolution plots a) and corresponding log-log plots b) for the Hamiltonian in equation (13), where the random variables are assigned according to a Gaussian distribution with fixed mean $E_A = 0$ and variance in the range $\sigma^2 \in [0.05,0.50]$.

For each value of σ^2, D_{hc} is an average of five realizations of the on-site energies, which minimizes computational errors.

To show that a sufficiently large value of σ^2 can induce a metal-to-insulator transition, we changed the variance in the larger interval $\sigma^2 \in [0.2,2.0]$. Figure 5 shows that the distance plots drop to smaller limiting values as the variance is increased and at $\sigma^2 = 2.0$, the plot drops to zero within the size of the simulation. In this last case, the spectral approach cannot establish the existence of extended states, which suggests that the system has transitioned to a localized behavior. The determination of an exact transition point in the transport behavior of a lattice with on-site energies assigned from a Gaussian distribution is not the focus of this work. Here, we simply note that for a Gaussian distribution with a fixed mean $E_A = 0$, changes in the variance significantly affect the behavior of the distance parameter. This is to be expected since, physically, the variance quantifies the deviation from the mean energy and can be interpreted as a type of disorder in the system. Note, however, that in this case, the spread of the Gaussian function represents a defect characteristic of the undoped crystal and is, therefore, similar to the Anderson-type disorder.

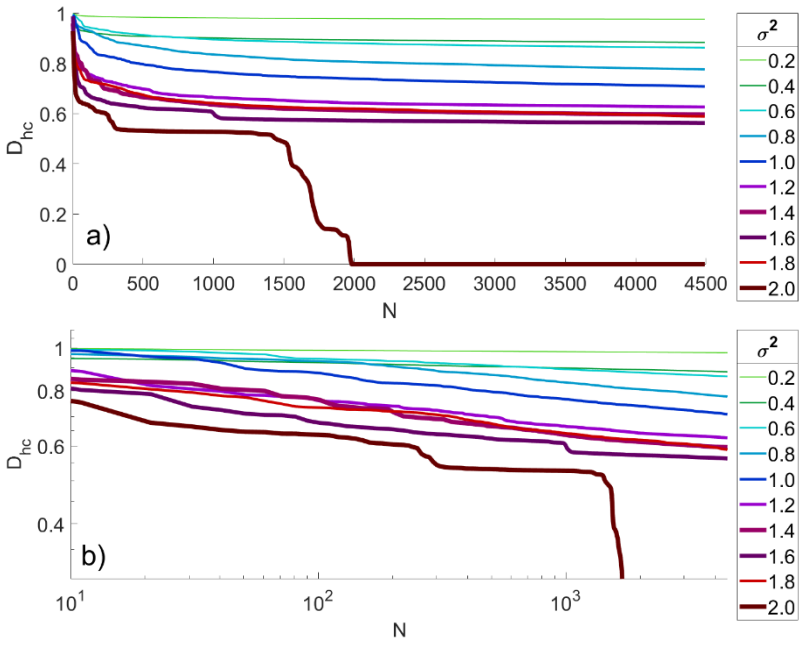

FIG. 5. Distance time evolution plots a) and corresponding log-log plots b) for the Hamiltonian in equation (13), where the random variables are assigned according to a Gaussian distribution with fixed mean $E_A = 0$ and variance in the range $\sigma^2 \in [0.2,2.0]$.

For each value of σ^2, D_{hc} is an average of five realizations of the on-site energies, which minimizes computational errors.

Although the focus of this work is substitutional defects, a realistic model of disorder should also account for lattice imperfections in the undoped crystal. Thus, it is useful to assume a value for σ^2 that contributes to the total effect of impurities but does not dominate it. Since the normal distribution models a type of defect which is similar to the Anderson-type disorder, we obtain an estimate for the appropriate value of σ^2 through comparison with our previous study [29], where we established that for the 2D honeycomb lattice with Anderson-type disorder (i.e., rectangular distribution), extended states exist for $W \leq 0.75$. In this study, it is important to choose a variance that corresponds to W smaller than this critical value.

An approximate relationship between the width of the square distribution W and the variance of the normal distribution σ^2 is presented in Fig. 6. Recall that $\approx 95\%$ of the area of the normal distribution falls within a distance 2σ from the mean, so it is standard to approximate the Gaussian by a square distribution with width $W = 4\sigma$ (light pink square in Fig. 6) or $W^2 = 16\sigma^2$. Therefore, the critical value $W \leq 0.75$ approximately corresponds to $\sigma^2 \leq 0.035$. The same calculation performed with a square of width 2σ (light blue square in Fig. 6) yields $\sigma^2 \leq 0.14$. Clearly, the pink square overestimates and the blue square underestimates the actual area of the Gaussian. Thus, it is appropriate to choose the variance from the range $0.035 < \sigma^2 < 0.14$.

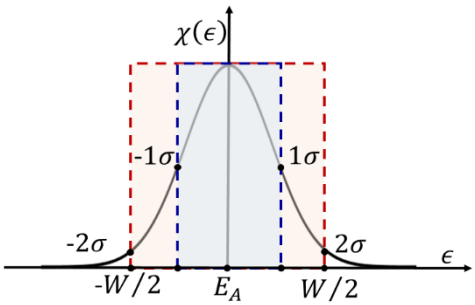

FIG.6. Visual representation of the connection between W for a square distribution and σ for a Gaussian distribution.

Based on the above, we chose $E_A = 0$ and $\sigma^2 = 0.05$ for the Gaussian peak of the modified bimodal distribution.

B. 2D honeycomb lattice with substitutional disorder

We now consider the modified bimodal distribution with a Gaussian peak (mean $E_A = 0$ and variance $\sigma^2 = 0.05$) and a delta function at $E_B = 100$. Here, $n_G = p$ is defined as the concentration of lattice sites with energy ϵ_i selected from the Gaussian peak and $n_D = 1 - p$ is defined as the concentration of lattice sites with energy $E_B = 100$. In each simulation, we assign on-site energies from the normal distribution to obtain a single-species crystal with small lattice imperfections. We then simulate substitutional disorder by randomly assigning the energy E_B to a fraction of the lattice sites determined by the value n_D. The doping concentration was varied over two ranges, corresponding to large doping, $n_D(\%) \in [1,32]$ and small doping $n_D(\%) \in [0,1)$. To reduce the effect of numerical errors, for each value of n_D, we generated multiple realizations (30 for large and 50 for small doping) of the on-site energies and then averaged the corresponding distance values.

1. Large variation of doping concentration

The time evolution of D_{hc} for $n_D(\%) = 1{:}\,1{:}\,10$, plotted in Fig. 7a, indicates that for doping as small as 2% the distance values show an observable drop from the undoped lattice case $n_D(\%) = 0$ (shown as a black dashed line on the graph). Similarly, the corresponding log-log plots exhibit increasingly negative slopes for $n_D(\%) \geq 0.2$, which suggests that these D_{hc} values do not flatten exponentially over the number of iterations in the present simulation. In addition, as the doping concentration increases, some realizations rapidly drop to zero, which results in sharp drops in the averaged distance plots (more visible as kinks in Fig. 7b). According to the spectral approach, the occurrence of such a realization (which we define as 'failures') indicates that delocalization cannot be established for the corresponding disordered system. Thus, the method suggests that for doping $n_D(\%) \geq 0.2$, the 2D honeycomb lattice has already transitioned into an insulating behavior, which agrees with experimental results. The consistency of these predictions is further supported by data shown in Fig. 7c, where the number of failed realizations is plotted as a function of increasing doping concentration in the range $11 \leq n_D(\%) \leq 32$.

Note that, even for the cases where all realizations for a given n_D have a positive value at the last timestep of the simulation, i.e., $D_{hc}(4500) > 0$, proof of existence of extended states requires examination of the limiting behavior as $N \to \infty$. To extrapolate $D_{hc}(N \to \infty)$, we fit the data using the equation

$$D_{hc} = mN^{-\alpha} + b, \tag{7}$$

where the first term shows how rapidly D_{hc} approaches a constant value b as $N \to \infty$. Since all plots exhibit small fluctuations over the first thousand timesteps, we apply a nonlinear fitting to equation (7) using a weight function of the form $w = 1/\sqrt{4500 - n}$. In this way, the fit to the initial data reduces the effect of fluctuations, and thus more accurately reflects the behavior at large N. To evaluate the contribution of the first term in equation (7), we define the ratio parameter

$$R = \frac{D_{hc}(4500) - b}{D_{hc}(4500)} \times 100\%, \tag{8}$$

which gives the percent contribution of the decaying term at the last timestep of the simulation.

Mathematically, showing that D_{hc} limits to *any* nonzero positive number (however small) is sufficient evidence for the existence of extended states with probability 1. However, due to the

finite character of the numerical simulations (restricted by the computation time), it is necessary to introduce a criterion for the maximum acceptable value for the ratio R. A rough estimation can be performed using the following physical reasoning. The chosen number of iterations, $N = 4500$, yields a lattice size of $\approx 4 \times 10^7$, which (using the average carbon-carbon bond length for graphene, $a \approx 0.142$ nm) corresponds to a sample of the 2D material with area $\approx 1\ \mu m^2$. The sizes of graphene flakes (currently available for industry) range from the nanometer scale to a few thousand squared microns depending on the substrate used [34], [35]. Thus, the simulations presented here reflect the behavior of a typical sample size for a two-dimensional material. It is therefore physically reasonable to require that numerical delocalization cannot be claimed if the ratio R contributes more than 10% of the computed distance parameter.

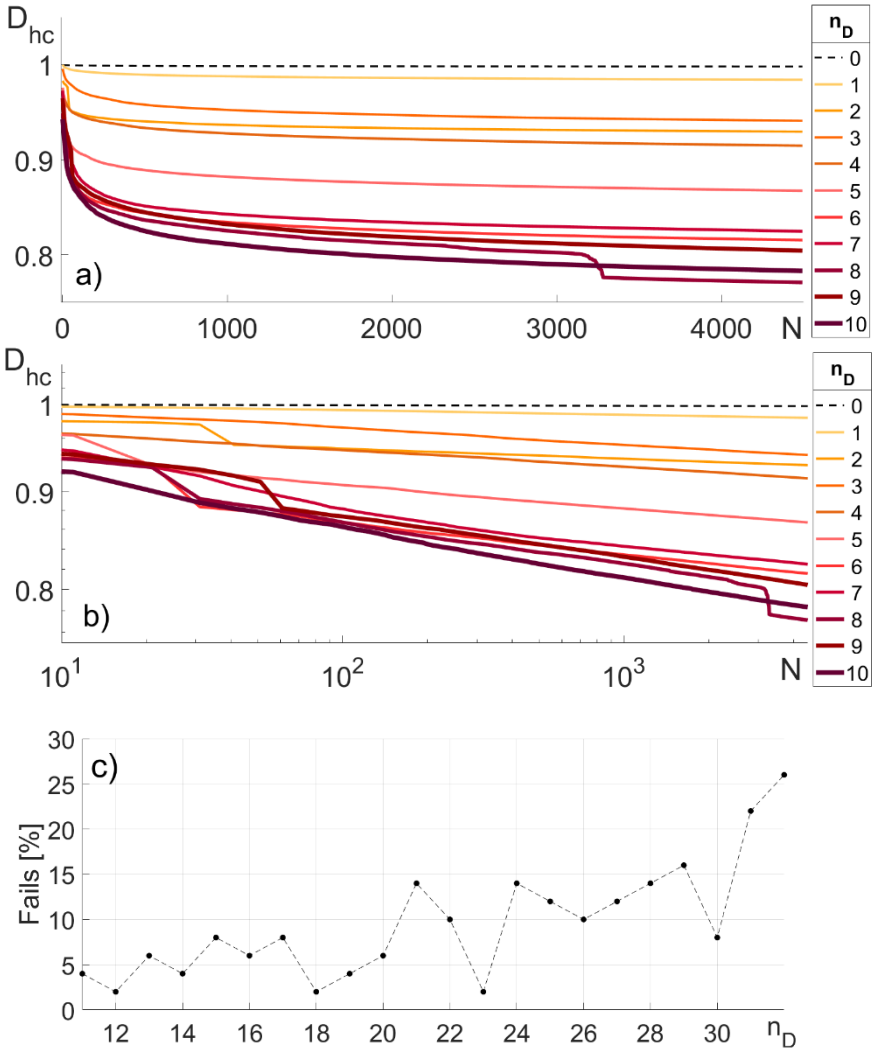

FIG. 7. Distance time evolution plots a) and the corresponding log-log plots b) for doping in the range $n_D(\%) = 1{:}\,1{:}\,10$. c) The number of realizations for which the distance dropped to zero for disorder in the range $n_D(\%) = 11{:}\,1{:}\,32$.

The values of b, $D(4500)$, and R corresponding to doping concentrations $n_D(\%) = 1{:}\,1{:}\,10$ are provided in Table I. Due to the presence of failed realizations in this range, the calculation of the parameters b and R were obtained by first averaging all realizations per doping value, and then

performing the equation fit[8]. In each case, the root mean squared error in the equation fitting analysis (showing the goodness of the fits) was $\lesssim 10^{-4}$. Comparison of columns two and three shows that, although the values of D_{hc} at the last timestep are positive for all concentrations, the limiting values b quickly drop and cross zero between $n_D(\%) = 5 - 6$. In addition, the contribution from the ratio R for doping concentration $n_D(\%) = 1$ is already 22%, confirming that for the size of the performed simulations, $n_D(\%) \geq 1$ is already too large to yield distance parameters that flatten out exponentially. This further suggests that the 2D honeycomb lattice in this regime is not characterized by metallic behavior.

TABLE I. Extrapolated values from equation fitting of averaged distance plots corresponding to doping $n_D(\%) = 0{:}\,1{:}\,10$.

$\boldsymbol{n_D}(\%)$	b	$D(4500)$	$R(\%)$
0	0.964	0.998	3%
1	0.772	0.984	22%
2	0.537	0.968	45%
3	0.309	0.941	67%
4	0.162	0.915	82%
5	0.050	0.911	94%
6	-0.263	0.874	130%
7	-0.074	0.825	109%
8	-0.767	0.857	190%
9	-0.824	0.843	198%
10	-0.770	0.783	198%

2. Small variation of doping concentration

The time evolution plots of the distance values obtained for the small doping range $n_D(\%) \in [0,1]$ are presented in Fig. 8a. For all concentrations, the averaged D_{hc} was obtained using at least 30 realizations of the disorder, which minimizes possible numeric artifacts. As can be seen, the plots corresponding to $n_D(\%) = 0.9$ and $n_D(\%) = 1$ drop much faster than the rest, which suggests dissimilarity in their behavior. Analysis of the individual realizations used to obtain these two (averaged) distance time evolutions shows that in both cases, there is at least one realization that rapidly dropped to zero. Thus, based on the analysis of the previous section, it is reasonable to expect that the transition in the transport behavior of the lattice occurs in the even smaller range $n_D(\%) \in [0,0.8]$. Figure 8b shows the log-log plots (solid lines) and the corresponding equation fits (dotted, dot-dashed, and dashed lines) obtained using equation (7). As expected, the slopes of the log-log plots become increasingly negative with increasing doping concentration, which indicates slower decay towards constant nonzero values.

[8] Alternatively, one can first perform a fit to each realization and then average the results, which will yield an error estimate (spread from the mean value) for b and R. However, such analysis is only possible if there are no realizations that rapidly fall to zero, which is not the case for large doping in our study. In the small doping regime explored in the next section, the results are confirmed using both fitting techniques.

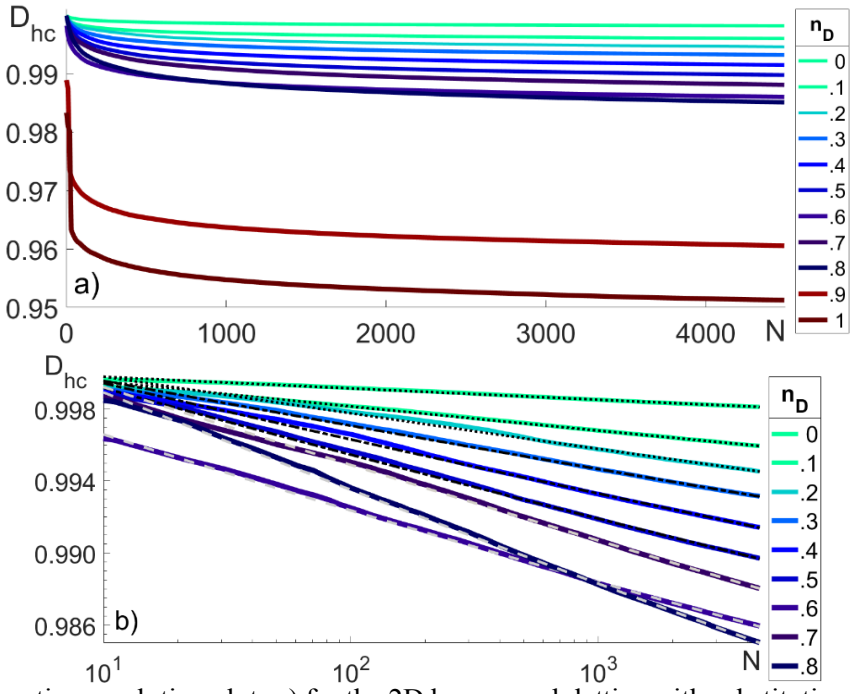

FIG. 8. Distance time evolution plots a) for the 2D honeycomb lattice with substitutional disorder in the range $n_D(\%) = 0{:}\ 0.1{:}\ 1$ and corresponding log-log plots b) for the range $n_D(\%) = 0{:}\ 0.1{:}\ 0.8$.

The averaged values for b, $D(4500)$, and R are given in Table II. As mentioned above, concentrations $n_D(\%) = 0.9$ and $n_D(\%) = 1$ each had at least one realization that rapidly dropped to zero, which, according to the spectral approach suggests an onset to localized behavior. Thus, the parameters for these cases were obtained by first averaging all of the realizations and then fitting to equation (7). In the smaller concentration range, $n_D(\%) \in [0{,}0.8]$, the values within parentheses reflect results from first performing the fits and then averaging, providing an error estimate based on the spread of the separate realizations. Although the two fitting techniques show agreement, the presence of outliers causes some differences in the values extrapolated for b and R. Since these outliers do not appear in a consistent manner as the concentration is increased (unlike the realizations that fall to zero for $n_D(\%) \geq 0.9$), it is not clear if they represent physically meaningful data or simply computational error. Thus, in this section we extrapolate b and R from the fits on the averaged distance values. A treatment that does not ignore outliers is presented in the next section, where the separate realizations are analyzed statistically.

For all cases considered, the root mean squared error[9] from the fit equation was $\sim 10^{-5}$, which indicates good agreement with the weighted equation fitting model. Table II shows that as doping concentration increases, the values of b decrease, and the contribution R becomes larger. For $n_D = 0.3$ (shaded row in Table II), the ratio R contributes 10% of the distance value obtained at the last timestep, which suggests a transition in the behavior of the D_{hc} plots.

[9] Note that there are two distinct errors in the discussion. The *error estimates* obtained from the spread of the random realizations for each disorder (the ones shown in Table II) indicate the certainty with which we can determine the limiting behavior of the distance values. The *root mean squared error* shows the goodness of the fit.

TABLE II. Extrapolated values from equation fitting of averaged distance plots corresponding to doping $n_D(\%) = 0{:}\,0.1{:}\,1$. The shaded row highlights the parameters for the critical value $n_D = 0.3\%$. The numbers in parentheses are the average and the standard deviation of each parameter based on the fits of individual realizations. As explained in the text, such analysis is only possible for the smaller range $n_D(\%) = 0{:}\,0.1{:}\,0.8$, where no D-values dropped to zero.

$\boldsymbol{n_D}(\%)$	b	$D(4500)$	$R(\%)$
0	0.958 (960 ± 10)	0.998 (998 ± 0)	4 (4 ± 1)
0.1	0.940 (942 ± 55)	0.996 (996 ± 4)	6 (5 ± 6)
0.2	0.920 (920 ± 58)	0.995 (995 ± 6)	8 (7 ± 6)
0.3	0.898 (881 ± 45)	0.993 (993 ± 5)	10 (9 ± 6)
0.4	0.877 (860 ± 30)	0.991 (991 ± 5)	12 (11 ± 5)
0.5	0.856 (850 ± 30)	0.990 (930 ± 6)	13 (13 ± 3)
0.6	0.837 (827 ± 31)	0.986 (986 ± 17)	15 (14 ± 3)
0.7	0.820 (796 ± 67)	0.988 (988 ± 5)	17 (16 ± 3)
0.8	0.800 (796 ± 67)	0.985 (985 ± 8)	19 (19 ± 7)
0.9	0.804	0.982	18
1	0.769	0.978	21

3. Statistical analysis for small doping[10]

To confirm the existence of a transition point in the range $n_D(\%) = 0{:}\,0.1{:}\,0.8$, we study the dissimilarity among the values extrapolated for b by equation fitting of the separate realizations for each concentration. The total number of observations in this range is 450 (i.e., 50 realizations per doping value). Figure 9 shows a dendrogram of the data obtained from hierarchical clustering algorithm with Ward's minimum variance method. Note that for clarity, the dendrogram consists of 30 leaves, where each leaf represents clusters of highly similar points. Figure 9 shows the existence of two distinct clusters, which we name 'small group' and 'large group'. These clusters correspond to two different regimes in the limiting behavior of the distance plots, and the transition from one to the other is interpreted as a transition in the transport properties of the lattice.

[10] For more details on the statistical tests applied to this data, see the supplementary material in [36].

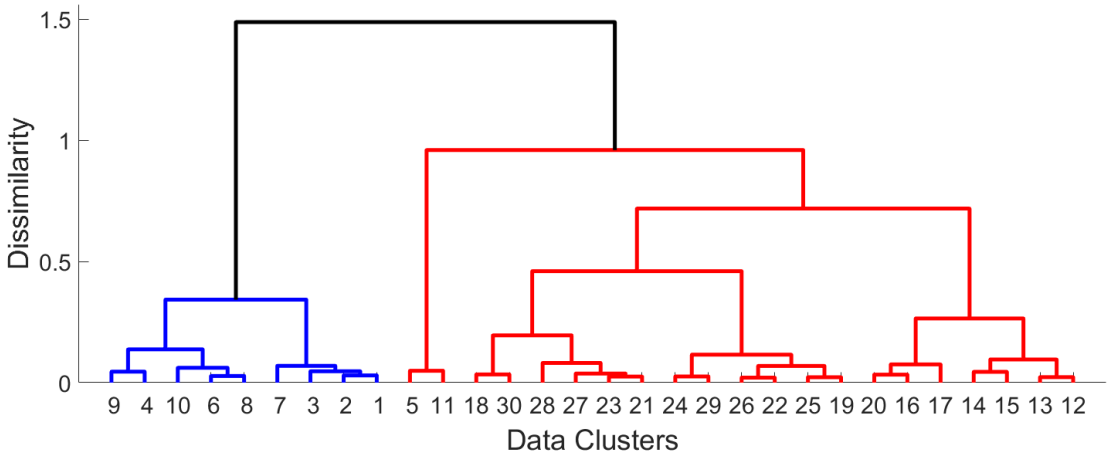

FIG. 9. Dendrogram for the averaged values of b for doping in the range $n_D(\%) = 0\colon 0.1\colon 0.8$. Each of the 30 leaves represents clusters of highly similar data points. The blue cluster represents the small group, while the red cluster corresponds to the large group.

Table III provides a classification of all examined b values according to the two groups identified by clustering analysis. Comparison of the percent contributions to each group indicates that the transition occurs as the doping increases from $n_D = 0.3\%$ to $n_D = 0.4\%$, at which doping level a considerable percentage of realizations belongs to both groups. Indeed, a hypothesis test confirms that the average value of b for doping levels from 0% to 0.3% inclusive is significantly different from the average value of b for doping levels of 0.4% to 0.8% inclusive (p-value < 0.001). Thus, we conclude that $n_D = 0.3\%$ marks the onset of the insulating behavior in the lattice, in agreement with the experimental results presented by Bostwick et al. [6]. From Table III we see that for doping values $n_D(\%) = 0.1, 0.2, \text{and } 0.6$, there is only one realization (or 2%) that lies in a different group, which is considered an outlier due to computational error.

TABLE III. Percentage of observations for each doping level that are assigned to the "small" or "large" group by Hierarchical Clustering using Ward's Distance, as shown in Fig. 9.

$n_D(\%)$	**0**	**0.1**	**0.2**	**0.3**	**0.4**	**0.5**	**0.6**	**0.7**	**0.8**
Small Group	100	98	98	78	20	0	2	0	0
Large Group	0	2	2	22	80	100	98	100	100

IV. CONCLUSIONS AND FUTURE WORK

A. Summary of results

In this work, we have used the spectral approach (first introduced by Liaw in [27]) to establish the existence of extended states in a 2D honeycomb lattice with substitutional and positional disorder. The examined transport problem is described by an Anderson-type Hamiltonian, where the transfer energy is represented by a constant nearest-neighbor interaction (tight-binding approximation), and the on-site energies are random variables assigned according to a predetermined probability distribution χ. The transfer energy V has been normalized to unity; thus, the energies discussed here are in units of V.

In our study, disorder has been assigned from a modified bimodal distribution consisting of a Gaussian peak and a delta-type peak. The variables assigned from the Gaussian peak represent the fluctuations in the on-site energies of the undoped crystal. Preliminary analysis of various normal distributions suggest that it is reasonable to use a Gaussian peak with mean $E_A = 0$ and variance $\sigma^2 = 0.05$. In all numerical simulations, we used a delta function peaked at $E_B \approx 100$ to represent the approximate energy of the doping atoms.

The doping concentration was varied between $n_D = 0\%$ and $n_D = 32\%$. For $n_D \geq 0.9\%$, the spectral approach does not establish delocalization. Thus, we conclude that in this range, the transport behavior of the system has transitioned into the localized regime. We applied an equation fitting model and hierarchical clustering for small concentrations of the doping, $n_D(\%) \in [0,0.8]$. The results indicate the existence of a transition point in the transport behavior of the system for $0.3\% \leq n_D \leq 0.4\%$. In other words, the 2D honeycomb lattice exhibits metallic behavior for doping concentrations smaller or equal to 0.3%, which agrees with experiments where a single graphene sheet is doped with atomic hydrogen [6].

B. Comparison between the spectral approach and scaling theory

In the introduction, we mentioned that finite-size scaling models (often adopted in the analysis of 2D transport problems) assume approximations that can give incomplete information about the energy states of the Hamiltonian H. When such models rely on eigenvector-eigenvalue analysis, the existence of extended states, or transport, is established as a limiting behavior of the density of discrete energy states. Although this approach is appropriate for the study of localization lengths and critical exponents, it cannot determine the existence of extended states from the absolutely continuous spectrum of H.

The spectrum of the Hamiltonian H is the set of all possible energy states that can be obtained if one measures the total energy of a quantum mechanical system. Since H is a linear operator, its spectrum has a standard decomposition in three parts:

i. Pure point (pp) spectrum – the set of all discrete energy states (eigenvalues) at which the described physical system exhibit localization,

ii. Absolute continuous (ac) spectrum – the set of all extended energy states at which the described physical system exhibit transport,

iii. Singular continuous (sc) spectrum – poorly behaved pieces, corresponding to energy states that are neither extended, nor exponentially localized.

Due to the presence of the intermediate sc spectrum part, it is not a trivial subject to establish delocalization as a limiting behavior of eigenvalues or localization as a limiting behavior of extended energy states. Finite-size scaling models commonly establish transport from the behavior of the eigenvalues, while ignoring possible contributions from the ac spectrum. For example, the original scaling theory [9] is based on the relationship between the Kubo-Greenwood formula and the eigenvalue response to perturbation of boundary conditions in a finite hypercube. The transport regime in this approach is obtained from computing eigenvalues and following their behavior as one extends the system by fitting multiple hypercubes together. Delocalization in such formulation is established once the eigenvalues are discrete but infinitely close to one another. Therefore, although this eigenvalue-based technique is appropriate for the study of localization lengths and rates of decay in the different localized regimes, it cannot detect the existence of extended states from the ac spectrum.

The spectral approach presented here is designed to identify the cases where extended states may exist but were not expected from theories relying on eigenvector-eigenvalue analysis (such as the scaling approach to the 2D Anderson localization problem). Specifically, it offers a mathematical test detecting the existence of extended energy states from the ac spectrum of the Hamiltonian. In this sense, the spectral technique does not necessarily contradict previous results regarding the behavior of discrete energy states from the pp or sc spectrum, but rather provides complementary information that is unattainable using eigenvalue-based techniques.

C. Numerical limitations of the spectral technique

A natural limitation of the numerical analysis is the finite character of each simulation, which does not allow us to calculate an exact value of D at $n = \infty$. Instead, we use equation fitting to extrapolate the limiting behavior. We cannot exclude the possibility of a very slow power-law decay that leads to *apparent* delocalized behavior due to the size of the simulation. The results from the present analysis can be improved by increasing the number of timesteps N. This will yield better estimates for the errors in the values of b and R, used to determine the existence of transitions in the transport behavior of the system. Further improvements of the present analysis will come from optimization of the parameters for the probability distribution χ so that specific application of 2D materials can be examined.

Another limitation of the proposed model is related to energy states corresponding to the singular or singular-continuous parts of the spectrum. In spectral theory, the distinction between the exponential and the power-law decay is represented by differences in the fine properties of the corresponding pure point component (i.e., "eigenvalues") of the energy spectrum. Throughout the literature, the different types of localization behavior are often connected with how fast "eigenfunctions" may be decaying. For example, exponentially and some fast power-law decaying functions may belong to the Hilbert space, in which case they are true eigenfunctions and the corresponding eigenvalues belong to the singular component of the spectrum. This would mean that such states appear as localized in the spectral method. Further, if the power-law decay is medium slow, then there is a chance that these "states" would belong to what is called the singular continuous spectrum. For even slower power-law decay, the resulting states can possibly be included in the absolutely continuous spectrum (commonly thought of as the conducting regime).

The spectral approach used in our work is based on results by Jaksic and Last [37], [38] that are only applicable to the continuous component of the spectrum. Thus, if the distance parameter D limits to a positive nonzero value as the timestep goes to infinity, it can be mathematically shown that transport in the form of extended energy states exists with probability 1. In contrast, if the time evolution plot of D drops to zero, we cannot state with certainty that the corresponding transport behavior is localized. In other words, as mentioned in the previous section, the present mathematical technique cannot be *rigorously* used to obtain information about the localized regime. However, we have established numerically that the distance parameters drop to zero faster as the amount of disorder is increased, which agrees with the notion that there are various regimes of localized behavior.

Similarly, in the transition regime, multifractal states can occur in the system dynamics, which imply strong fluctuations on a subset of sites. We expect that these states belong to the singular or singular-continuous component of the spectrum. Thus, much like the power-law decaying states, the multifractal ones cannot be rigorously identified with the present spectral method. However, we expect that the distance functions will drop to zero for the multifractal states and that the

SPEED of decay of the distance function for a given multifractal state will differ from the states that are localized more strongly. We are currently working on an improved physical interpretation of the spectral technique, which should be used to justify the application of the method to the localized regime.

C. Future directions for research

A particularly interesting direction for future work is the examination of systems, characterized by nonlocal interactions. One way to model such systems is to consider lattices with dimerized defects, in which the doping type-B atoms are inserted in neighbor pairs in the lattice of type-A atoms. The use of dimerized defects in numerical simulations aims to model systems with short- or long-range correlated disorder. The presence of such correlations has been suggested as a possible mechanism guiding the metal-to-insulator transition (MIT) in low-dimensional systems [39]. As the spectral approach is independent of the choice of probability distribution function for the on-site energies, one can simulate correlated disorder by modifying the properties of the PDF.

Another approach to the study of nonlocal interactions is to consider systems characterized by anomalous diffusion. It has been shown [40], [41] that the non-local characteristics of anomalous diffusion can be modeled using a fractional Laplacian operator $(-\Delta)^s$, where $0 < s < 2$. It is expected that in the subdiffusive regime ($s > 1$) the propagation through the medium slows down due to negative correlations, while for $s < 1$, transport is enhanced due to positive correlations. In a future project we will examine how the interplay between disorder type and diffusion regime affects the dynamical behavior of low-dimensional systems.

ACKNOWLEDGMENTS

This work was supported by the NSF-DMS (grant number 1802682, C D L), NASA grant number 1571701 and NSF grant numbers 1414523, 1740203, 1262031 (L S M and T W H).

APPENDIX

Here we provide a discussion of spectral theory and its application to transport problems. The basic steps in the spectral method are introduced for the specific case of a disordered 2D honeycomb lattice Λ (Fig. 10), characterized by the discrete random Schrödinger operator. It is important to note, however, that the spectral approach can be applied to the entire class of Anderson-type Hamiltonians (first introduced in [38]) and generalized to any dimension or geometry.

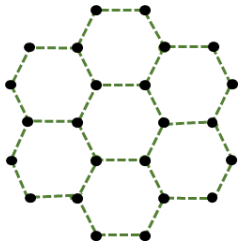

FIG. 10. Honeycomb lattice Λ, where black dots represent lattice vertices and dashed lines represent

1. Spectral decomposition of the Hamiltonian

The 2D honeycomb lattice Λ is the graph $G = (V, E)$ of the 2D set of vertices (or sites) $\{\mathrm{v}_i\}$ connected by edges (or bonds) $\{\mathrm{e}_{ij}\}$. Bonds represent the graph distance between pairs of nearest neighbors (i.e., vertices located at a Euclidean distance 1 apart from each other). For any function

of the vertices $f(\mathrm{v}_i)$ taking values in the 2D set of all integers Λ, the (discrete) Laplacian acting on f is given by

$$\Delta f = \sum_{\mathrm{e}_{ij}=1} \left[f(\mathrm{v}_i) - f(\mathrm{v}_j) \right], \tag{9}$$

where e_{ij} is the edge between vertices v_i and v_j, and the sum is over the nearest neighbors of vertex v_i. Thus, we see that the discrete Laplacian Δ is the graph representation of the hopping amplitude term in equation (1).

Let $l^2(\Lambda)$ be the Hilbert space of square-summable sequences on the 2D space Λ. In this case, the graph representation of the Hamiltonian given in equation (1) is the discrete random Schrödinger operator on $l^2(\Lambda)$

$$H_\epsilon = -\Delta + \sum\nolimits_{i \in \Lambda} |e_i\rangle \epsilon_i \langle e_j|, \tag{10}$$

where $\epsilon_i \in [a, b]$ are defined as in Sec. II A and the set of base vectors $|e_i\rangle$ now represents the vertices of the discrete lattice Λ. Without loss of generality, assume that the interval of possible on-site energies has a width W and is symmetric about the origin, i.e., $\epsilon_i \in [-W/2, W/2]$. Thus, the value of the parameter W can be used to vary the amount of disorder in the crystal. The random Schrödinger operator given in (10) models a honeycomb lattice comprised of atoms located at the vertices.

The spectral approach uses the Spectral Theorem to diagonalize the Hamiltonian and obtain its energy spectrum. The Spectral Theorem maps the square summable Hilbert space $l^2(\Lambda)$ to a new space $L^2(\mu)$, consisting of the square-integrable functions with respect to the spectral measure μ. This new space $L^2(\mu)$ can be decomposed into two orthogonal Hilbert spaces, $L^2(\mu_{ac})$ and $L^2(\mu_{sing})$, where the spectral measure μ is decomposed into an absolutely continuous part and a singular part

$$\mu = \mu_{ac} + \mu_{sing}. \tag{11}$$

The energy spectrum of the Hamiltonian therefore has a singular part $(H_\epsilon)_{ac}$ that comes from $L^2(\mu_{ac})$ (representing the extended states) and a part $(H_\epsilon)_{sing}$ that comes from $L^2(\mu_{sing})$ (roughly speaking, corresponding to localized states). It was shown [38] that cyclicity of vectors in $l^2(\Lambda)$ is related to the singular part of the spectrum and that non-cyclicity of any vector in the same space indicates the existence of an absolutely continuous part of the spectrum.

Theorem [42]: For any *nonzero* vector v_0[11] in the lattice space $l^2(\Lambda)$, v_0 is cyclic for the singular part $(\mathrm{H}_\epsilon)_{\mathrm{sing}}$ with probability 1.

Theorem [27]: If one shows that v_0 is *not* cyclic for H_ϵ with non-zero probability, then almost surely [12]

[11] Note that, in this section, a vertex v_i is the graph analogue of a base vector $|e_i\rangle$ while v_i is any vector in the space (i.e. v_i is a linear combination of the chosen base vectors).

[12] Note that in probability theory an event happens *almost surely* if it happens *with probability* 1. In this paper, we use the two phrases interchangeably.

$$H_\epsilon \neq (H_\epsilon)_{sing}, \tag{12}$$

which indicates the existence of extended states since H_ϵ must have a non-zero absolutely continuous part.

2. Spectral approach

For a given realization of the disorder in the 2D honeycomb lattice:

(i) Fix a random vector, say v_0, in the 2D space $l^2(\Lambda)$, and generate the sequence $\{v_0,\ H_\epsilon v_0,\ (H_\epsilon)^2 v_0,\ \cdots, (H_\epsilon)^N v_0\}$ where $N \in \{0,1,2,\dots\}$ is the number of iterations of H_ϵ and is used as a timestep.

(ii) Apply a Gram-Schmidt orthogonalization process (without normalization) to the members of the sequence, and denote the new sequence $\{m_0, m_1, m_2, \dots, m_N\}$.

(iii) Calculate the distance from *another* vector in the lattice space, say v_1, to the N-dimensional orthogonal subspace $\{m_0, m_1, m_2, \dots, m_N\}$, given by [27]

$$D^N_{\epsilon,W} = \sqrt{1 - \sum_{k=0}^{N} \frac{\langle m_k | v_1 \rangle^2}{\|m_k\|_2^2}}, \tag{13}$$

where $\|\cdot\|_2$ is the Euclidean norm and $\langle \cdot \mid \cdot \rangle$ is the inner product in the space. It can be shown [27], [33] that if for any v_1 (with nonzero probability) the limiting behavior of the distance vector obeys

$$\lim_{N\to\infty} D^N_{\epsilon,W} > 0, \tag{14}$$

then extended states exist with probability 1.

To ensure accuracy of the numerical results, we perform an orthogonality check on the sequence $\{m_0, m_1, m_2, \dots, m_N\}$, which indicates that the obtained vectors are indeed orthogonal, i.e., there is no Gram-Schmidt instability in the algorithm. A discussion on the orthogonality check procedure can be found in [29].

BIBLIOGRAPHY

[1] A. K. Geim and K. S. Novoselov, The rise of graphene, Nat. Mater. 6,183 (2007).

[2] K. S. Novoselov, D. Jiang, F. Schedin, T. J. Booth, V. V. Khotkevich, S. V. Morozov, and A. K. Geim, Two-dimensional atomic crystals, Proc. Natl. Acad. Sci. U. S. A 102, 10451 (2005).

[3] C. M. Chandrashekar and T. Busch, Quantum percolation and transition point of a directed discrete-time quantum walk, Sci. Rep. 4, 6583, (2014).

[4] S. Das Sarma, M. P. Lilly, E. H. Hwang, L. N. Pfeiffer, K. W. West, and J. L. Reno, Two-Dimensional Metal-Insulator Transition as a Percolation Transition in a High-Mobility Electron System, Phys. Rev. Lett. 94, 136401, (2005).

[5] S. Y. Zhou, D. A. Siegel, A. V. Fedorov, and A. Lanzara, Metal to Insulator Transition in Epitaxial Graphene Induced by Molecular Doping, Phys. Rev. Lett. 101, 086402 (2008).

[6] A. Bostwick, J. L. McChesney, K. V. Emtsev, T. Seyller, K. Horn, S. D. Kevan, and E. Rotenberg, Quasiparticle Transformation during a Metal-Insulator Transition in Graphene, Phys. Rev. Lett. 103, 056404 (2009).

[7] S. Agnoli and M. Favaro, Doping graphene with boron: a review of synthesis methods, physicochemical characterization, and emerging applications, J. Mater. Chem. A 4, 5002 (2016).
[8] P. W. Anderson, Absence of Diffusion in Certain Random Lattices, Physicsl Rev. 109, (1958).
[9] E. Abrahams, P. Anderson, D. Licciardello, and T. Ramakrishnan, Scaling theory of localization, Physicsl Rev. Lett. 42, (1979).
[10] P. A. Lee and D. S. Fisher, Anderson Localization in Two Dimensions, Phys. Rev. Lett. 47, 882 (1981).
[11] J. E. Barrios-Vargas and G. G. Naumis, Critical wavefunctions in disordered graphene, J. Phys. Condens. Matter 24, 255305 (2012).
[12] E. Amanatidis, I. Kleftogiannis, D. E. Katsanos, and S. N. Evangelou, Critical level statistics for weakly disordered graphene, J. Phys. Condens. Matter 26, 155601 (2014).
[13] V. I. Fal'ko and K. B. Efetov, Statistics of prelocalized states in disordered conductors, Phys. Rev. B 52, 17413 (1995).
[14] K. Nomura, M. Koshino, and S. Ryu, Topological Delocalization of Two-Dimensional Massless Dirac Fermions, Phys. Rev. Lett. 99, 146806, (2007).
[15] J. H. Bardarson, J. Tworzydło, P. W. Brouwer, and C. W. J. Beenakker, One-Parameter Scaling at the Dirac Point in Graphene, Phys. Rev. Lett. 99, 106801, (2007).
[16] T. Odagaki, N. Ogita, and H. Matsuda, Quantal percolation problems, J. Phys. C Solid State Phys. 13, 189 (1980).
[17] C. M. Soukoulis and G. S. Grest, Localization in two-dimensional quantum percolation, Phys. Rev. B 44, 4685 (1991).
[18] Y. Avishai and J. M. Luck, Quantum percolation and ballistic conductance on a lattice of wires, Phys. Rev. B 45, 1074 (1992).
[19] A. Mookerjee, I. Dasgupta, and T. Saha, Quantum percolation, Int. J. Mod. Phys. B 9, 2989 (1995).
[20] M. F. Islam and H. Nakanishi, Localization-delocalization transition in a two-dimensional quantum percolation model, Phys. Rev. E 77, 061109 (2008).
[21] H. N. Nazareno, P. E. de Brito, and E. S. Rodrigues, Quantum percolation in a two-dimensional finite binary alloy: Interplay between the strength of disorder and alloy composition, Phys. Rev. B 66, 012205 (2002).
[22] A. Eilmes, R. A. Römer, and M. Schreiber, Exponents of the localization lengths in the bipartite Anderson model with off-diagonal disorder, Phys. B Condens. Matter 296, 46 (2001).
[23] D. Daboul, I. Chang, and A. Aharony, Series expansion study of quantum percolation on the square lattice, Eur. Phys. J. B - Condens. Matter Complex Syst. 16, 303 (2000).
[24] V. Srivastava and M. Chaturvedi, New scaling results in quantum percolation, Phys. Rev. B 30, 2238 (1984).
[25] D. E. Khmelnitskii, Anderson Localization in a flow structure, JETP Lett 32, 229 (1980).
[26] B. Shapiro, Renormalization-Group Transformation for the Anderson Transition, Phys. Rev. Lett 48, 823 (1982).
[27] C. Liaw, Approach to the Extended States Conjecture, J. Stat. Phys., 1022 (2013).
[28] E. G. Kostadinova, C. D. Liaw, L. S. Matthews, and T. W. Hyde, Physical interpretation of the spectral approach to delocalization in infinite disordered systems, Mater. Res. Express 3, 125904 (2016).

[29] E. G. Kostadinova, K. Busse, N. Ellis, J. Padgett, C. D. Liaw, L. S. Matthews, and T. W. Hyde, Delocalization in infinite disordered two-dimensional lattices of different geometry, Phys. Rev. B 96, 235408 (2017).
[30] S. Kirkpatrick and T. P. Eggarter, Localized States of a Binary Alloy, Phys. Rev. B 6, 3598 (1972).
[31] G. Schubert and H. Fehske, Dynamical aspects of two-dimensional quantum percolation, Phys. Rev. B 77, 245130 (2008).
[32] L. Gong and P. Tong, Localization-delocalization transitions in a two-dimensional quantum percolation model: von Neumann entropy studies, Phys. Rev. B 80, 174205 (2009).
[33] W. King, R. C. Kirby, and C. Liaw, Delocalization for the 3-D discrete random Schroedinger operator at weak disorder, J. Phys. Math. Theor. 47, 305202, (2014).
[34] Graphene Industries -> Products [Online]. Available: http://grapheneindustries.com/?Products. [Accessed: 11-Jul-2018].
[35] F. V. Kusmartsev, W. M. Wu, M. P. Pierpoint, and K. C. Yung, Application of Graphene Within Optoelectronic Devices and Transistors, in Applied Spectroscopy and the Science of Nanomaterials, (Springer, Singapore, 2015), pp. 191–221.
[36] See Supplemental Material at [URL will be inserted by publisher] for the statistical tests applied to the data in this paper.
[37] V. Jakšić and Y. Last, Simplicity of singular spectrum in Anderson-type Hamiltonians, Duke Math. J. 133, 185 (2006).
[38] V. Jakšić and Y. Last, Spectral structure of Anderson type Hamiltonians, Invent. Math. 141, 561 (2000).
[39] F. M. Izrailev, A. A. Krokhin, and N. M. Makarov, Anomalous localization in low-dimensional systems with correlated disorder, Phys. Rep. 512, 125 (2012).
[40] V. V. Uchaikin, Self-similar anomalous diffusion and Levy-stable laws, Phys.-Uspekhi 46, 821, (2003).
[41] Ó. Ciaurri, L. Roncal, P. R. Stinga, J. L. Torrea, and J. L. Varona, Fractional discrete Laplacian versus discretized fractional Laplacian, ArXiv:150704986.
[42] E. Abakumov, C. Liaw, and A. Poltoratski, Cyclicity in rank-1 perturbation problems, J. Lond. Math. Soc. 88, 523 (2013).